A multi-million-year-old record of Greenland vegetation and glacial history preserved in sediment beneath 1.4 km of ice at Camp Century

Andrew J Christ, Paul R Bierman, Joerg M Schaefer, Dorthe Dahl-Jensen, Jørgen P Steffensen, Lee B Corbett, Dorothy M Peteet, Elizabeth K Thomas, Eric J Steig, Tammy M Rittenour, et al.

PNAS
www.pnas.org

Main Manuscript for

A multi-million-year-old record of Greenland vegetation and glacial history preserved in sediment beneath 1.4 km of ice at Camp Century

Andrew J. Christ*[1,2], Paul R. Bierman[1,2,3], Joerg M. Schaefer[4], Dorthe Dahl-Jensen[5,6], Jørgen P. Steffensen[5], Lee B. Corbett[1], Dorothy M. Peteet[4,7], Elizabeth K. Thomas[8], Eric J. Steig[9], Tammy M. Rittenour[10], Jean-Louis Tison[11], Pierre-Henri Blard[11,12], Nicolas Perdrial[1], David P. Dethier[13], Andrea Lini[1], Alan J. Hidy[14], Marc W. Caffee[15,16], John Southon[17]

[1] Department of Geology, University of Vermont, Burlington, VT 05405, USA
[2] Gund Institute for Environment, University of Vermont, Burlington, VT, 05405, USA
[3] Rubenstein School of the Environment and Natural Resources, University of Vermont, Burlington, VT, 05405, USA
[4] Lamont Doherty Earth Observatory, Columbia University, Palisades, NY 10964, USA
[5] Centre for Ice and Climate, PICE, Niels Bohr Institute, University of Copenhagen, 2200 Copenhagen, Denmark
[6] Centre for Earth Observation Science, University of Manitoba, Winnipeg, MB R3T 2N2 Canada
[7] NASA/Goddard Institute for Space Studies, NY, NY 10025, USA
[8] Department of Geology, University at Buffalo, Buffalo, NY 14260, USA
[9] Department of Earth and Space Sciences, University of Washington, Seattle, WA 98105, USA
[10] Department of Geosciences, Utah State University, Logan, UT 84322, USA
[11] Laboratoire de Glaciologie, DGES-IGEOS, Université Libre de Bruxelles, Brussels 1050 Bruxelles, Belgium
[12] Centre de Recherches Pétrographiques et Géochimiques (CRPG), CNRS, Université de Lorraine, 54500 Nancy, France
[13] Department of Geosciences, Williams College, Williamstown, MA 01267, USA
[14] Center for Accelerator Mass Spectrometry, Lawrence Livermore National Laboratory, Livermore, CA 94550, USA
[15] Department of Physics and Astronomy, Purdue University, West Lafayette, IN 47907, USA
[16] Department of Earth, Atmospheric, and Planetary Sciences, Purdue University, West Lafayette, IN 47907, USA
[17] Keck Carbon Cycle AMS Laboratory, Department of Earth System Science, University of California, Irvine, CA 92697-3100, USA

*Correspondence to Andrew Christ

Email: Andrew.Christ@uvm.edu

Andrew Christ	0000-0003-0989-6491
Paul Bierman	0000-0001-9627-4601
Joerg Schaefer	0000-0002-6358-7115
Dorthe Dahl-Jensen	0000-0002-1474-1948
Jorgen Steffensen	0000-0002-5516-1093
Lee Corbett	0000-0001-6224-8034
Dorothy Peteet	0000-0003-3029-7506
Elizabeth Thomas	0000-0002-6489-7123
Eric Steig	0000-0002-8191-5549
Tammy Rittenour	0000-0003-1925-0395
Jean-Louis Tison	0000-0002-9758-3454
Pierre-Henri Blard	0000-0002-8455-8014
Nico Perdrial	0000-0002-0308-3708
David Dethier	0000-0001-7501-1810
Andrea Lini	0000-0002-2920-570X
Alan Hidy	0000-0003-2916-1425
Marc Caffee	0000-0002-6846-8967
John Southon	0000-0001-6168-6235

Classification

Physical - Earth, Atmospheric, and Planetary Sciences

Keywords

Pleistocene; ice core; Arctic; climate; ice sheet

Author Contributions

Conceptualization: A.J. Christ, P.R. Bierman. Formal analysis: A.J. Christ, L.B. Corbett, D.M. Peteet, E.K. Thomas, J.M. Schaefer, E.J. Steig, T.M. Rittenour, J-L. Tison, P-H. Blard, N. Perdrial, D. Dethier, A. Lini, A.J. Hidy, M. Caffee, J. Southon. Resources: D. Dahl-Jensen, J.P. Steffensen. Visualization: A.J. Christ, D.M. Peteet, N. Perdrial, J-L. Tison, P-H Blard. Writing – original draft: A.J. Christ, P.R. Bierman. Writing – review & editing: J.M. Schaefer, L.B. Corbett, D.M. Peteet, E.K. Thomas, E.J. Steig, T.M. Rittenour, J-L Tison, P-H Blard, D. Dahl-Jensen, J.P. Steffensen, N. Perdrial, D. Dethier, A.J. Hidy, M.W. Caffee, J. Southon.

This PDF file includes:

Main Text
Figures 1 to 4

Abstract

Understanding the history of the Greenland Ice Sheet (GrIS) is critical for determining its sensitivity to warming and contribution to sea level; before the last interglacial that history is poorly known. Most knowledge comes from interpretation of marine sediment, an indirect record of past ice-sheet extent and behavior. Sub-glacial sediment and rock, retrieved at the base of ice cores, provide terrestrial evidence for GrIS behavior during the Pleistocene. Here, we use multiple methods to determine GrIS history from sub-glacial sediment at the base of the Camp Century ice core, collected in 1966. This material contains a stratigraphic record of glaciation and vegetation in northwestern Greenland spanning the Pleistocene. Enriched stable isotopes of pore-ice suggest precipitation at lower elevations that imply ice-sheet absence. Plant

macrofossils and biomarkers in the sediment indicate that paleo-ecosystems from previous interglacial periods are preserved beneath the GrIS. Cosmogenic $^{26}Al/^{10}Be$ and luminescence data bracket the burial of the lower-most sediment between <3.2 ± 0.4 Ma and >0.7-1.4 Ma. In the upper-most sediment, cosmogenic $^{26}Al/^{10}Be$ data require exposure within the last 1.0 ± 0.1 Ma. The unique sub-glacial sedimentary record from Camp Century documents at least two episodes of ice-free, vegetated conditions, each followed by glaciation. The lower sediment derives from an Early Pleistocene GrIS advance. $^{26}Al/^{10}Be$ ratios in the upper-most sediment match those in sub-glacial bedrock from central Greenland, suggesting similar ice-cover histories across the GrIS. We conclude that the GrIS persisted through much of the Pleistocene but melted and re-formed at least once since 1.1 Ma.

Significance Statement

Understanding Greenland Ice Sheet history is critical for predicting its response to future climate warming and contribution to sea-level rise. We analyzed sediment at the bottom of the Camp Century ice core, collected 120 km from the coast in northwestern Greenland. The sediment, frozen under nearly 1.4 kilometers of ice, contains well-preserved fossil plants and biomolecules sourced from at least two ice-free warm periods in the past few million years. Enriched stable isotopes in pore ice indicate precipitation at lower elevations, implying ice-sheet absence. The similarity of cosmogenic isotope ratios in the upper-most sediment to those measured in bedrock near the center of Greenland suggests that the ice sheet melted and re-formed at least once during the past million years.

Introduction

The history of the Greenland Ice Sheet (GrIS) and the ecosystems that occupied Greenland during ice-free intervals are poorly known before the Last Glacial Maximum, and particularly prior to the last interglacial. Most evidence is drawn from marine sediments (1–5), geophysical surveys (6), a few terrestrial deposits (7, 8), and ice-core basal materials (9–12). Because well-dated terrestrial sediment archives are lacking, much of GrIS history is based on offshore records that provide only indirect constraints on ice-sheet extent and terrestrial ecosystems. This fragmentary knowledge of Greenland's climate history limits our understanding of ice-sheet and ecosystem sensitivity to climate warming.

Knowledge of Greenland glacial history and ecosystems is limited for periods older than ~1 Ma, and in most cases only glaciation more extensive than present can be directly constrained. Ice-rafted debris (IRD) in marine sediment indicates that Greenlandic glaciers reached the ocean possibly as early as 45 Ma (13) but certainly by 7.5 Ma (1). Ice cover grew substantially at 3.3 Ma (14) and culminated in an expanded GrIS by 2.7 Ma (1). Cosmogenic isotopic analyses of IRD and other glacial-marine sediment suggest that glacial erosion began stripping the pre-glacial landscape by 7 Ma and had eroded most shallow regolith by 1.8-2.0 Ma (2, 15). Charcoal and organic debris in outwash near the Hiawatha Crater (16) and pollen in marine sediment in Baffin Bay and the Labrador Sea indicates that boreal forests in humid, cool-temperate to sub-Arctic climate during the Late Pliocene transitioned to tundra vegetation in a cold polar climate during the Early Pleistocene (17, 18). Seismic-reflection surveys record multiple GrIS advances to the edge of the continental shelf in Melville Bay after 2.7 Ma (6). Although poorly dated, rare fossil-rich shallow-marine and coastal sediments overlying glacial deposits document warm, forested conditions that imply a smaller GrIS for short (<20 kyr) periods between ~2.4 and ~1.8 Ma (7, 8).

Ice-sheet behavior is better known for the past million years because of analyses of ice-core basal materials sourced from landscapes covered by the present GrIS (Fig 1). In central Greenland, silty ice at the base of the GRIP ice core is as old as 950 or 970 ka (9, 19). In the nearby GISP2 ice core, stratigraphic reconstructions and $\delta^{40}Ar$ dating suggest that the deepest

ice is older than 200 ka (20, 21). Silty ice in GISP2 preserves material from a pre-glacial landscape, which suggests persistent, non-erosive ice cover during much of the Pleistocene (11). Cosmogenic $^{26}Al/^{10}Be$ data from bedrock in west Greenland (22) and beneath the GISP2 ice core (10) require that ice disappeared from central Greenland at least once within the past 1.1 Myr. Marine sediment records suggest an ice-free and forested southern Greenland during Marine Isotope Stage (MIS) 11 (374-424 ka) (3, 4), while DNA studies of DYE-3 basal ice found flora and fauna from some time between 450 and 800 ka (9). Preservation of ice from MIS 5e (119 – 127 ka) in all Greenland deep ice cores (9, 12, 19–21, 23, 24), minimal ice-surface lowering at NEEM (12) at that time, sediment flux from southern Greenland (25), and coupled climate-ice sheet models (26) all indicate that the GrIS remained largely intact during the last interglacial. Except for DYE-3 and Camp Century, all ice cores have been collected from Greenland's interior. Less is known about GrIS extent, behavior, and stability near its margins, the portions of the ice sheet that will melt first and contribute the most to sea level rise under future warming scenarios (27).

The Camp Century ice core, collected from the ice-sheet periphery in northwestern Greenland, recovered 3.44 m of frozen sediment from beneath 1368 m of glacial ice and 14 m of silty ice (28); this is the thickest sub-glacial sedimentary archive recovered from a Greenland ice core (Fig 1B, 2A). Collected in 1966, the sub-glacial sediment was not studied beyond initial reports of sediment provenance (29) and microfossils, including abundant freshwater diatoms and chrysophyte cysts, pollen and scarce marine fossils (likely wind-blown), such as diatoms, sponge spicules and dinoflagellates (30). The basal material remained in frozen storage for decades until it was rediscovered in 2017.

Here, we decipher the glacial and ecological history of northwestern Greenland using analytical techniques that were unavailable when this unique sediment archive was retrieved over 50 years ago. We analyzed two samples, respectively from the upper- and lower-most sections of the Camp Century sub-glacial sediment. We determine the depositional history and characteristics of the sediment using *in situ* cosmogenic nuclides, infrared-stimulated luminescence (IRSL), geochemistry, light microscopy, and scanning electron microscopy and energy dispersive X-ray spectroscopy (SEM-EDS) analyses. We infer weathering conditions, paleo-elevation, and paleoclimate from pore-ice composition, and we characterize the paleoecology from macrofossil vegetation and biomarkers. We find that the Camp Century sub-glacial sediment preserves a unique, multi-million-year-old record of glaciation and vegetation. These data are consistent with persistent ice cover interrupted by at least two periods of ice-sheet loss and re-growth, once in the Early Pleistocene and another in the past 1.1 Myr.

Results

The Camp Century sub-glacial sediment includes two distinct units of frozen diamicton separated by an intermediate layer of debris-rich ice (Fig 2A, SI Text). Permafrost features such as sub-horizontal ice lenses are present only in the lower and intermediate unit. The contact between the intermediate ice layer and the upper diamicton is non-conformable and angular. The two samples we analyzed are from the upper (1059-4) and lower (1063-7) diamicton units (Fig 2B-C). Both diamictons contain a variety of lithologies, but the mineralogy is primarily quartz with few feldspars and mafic minerals. The lower sample contains a greater percentage of fine sediment (<125 μm) (Figs. 2A, S1, SI includes full description). Pore-ice major ion chemistry and SEM-EDS analysis of grain coatings indicate greater chemical weathering in the lower sample than the upper sample (Figs. 2D-E, S2, Table S1).

Cosmogenic $^{26}Al/^{10}Be$ ratios and IRSL confirm that the upper and lower samples have different histories of exposure and burial (Fig 2F, Tables S2-8). *In situ* ^{10}Be and ^{26}Al are produced in quartz during near-surface exposure to cosmic rays, and when buried, radioactively decay at different rates over time. Relatively low ^{10}Be concentrations and $^{26}Al/^{10}Be$ ratios less than that expected from surface production (7.3) indicate long burial with limited exposure before or during the burial period (31) (see SI Text for complete details). The $^{26}Al/^{10}Be$ ratio in the upper sample

(4.5 ± 0.3, n = 6, average ± standard deviation, weighted by $^{26}Al/^{10}Be$ measurement uncertainty) requires exposure within the past 1.0 ± 0.1 Myr, while $^{26}Al/^{10}Be$ in the lower sample (1.8 ± 0.4, n = 3) indicates longer burial, but no more than 3.2 ± 0.4 Myr (Fig 2F, Table S8). Multiple feldspar luminescence dating approaches indicate the lower sample was last exposed to sunlight before 0.7-1.4 Ma (Fig S3, Tables S9-10). The upper sample did not produce meaningful IRSL results due to light exposure during storage and sub-sampling.

Sediment pore-ice stable isotopes are enriched in both samples, which require precipitation at elevations lower than the present ice-surface elevation at Camp Century (1890 meters above sea level) and imply ice-sheet absence (Table S11). Pore-ice $\delta^{18}O$ values are 5.9 ‰ to 7.5 ‰ greater than mean Late Holocene precipitation (–29‰) at Camp Century (23), which can be explained by both lower surface elevation and possibly warmer temperatures than present. For example, removal of the present ice sheet (thickness of 1382 m) at Camp Century and isostatic adjustment would raise the current bedrock elevation by ~440 m, implying a net surface elevation lowering of ~950 m. Such an elevation change would account for 5.3 ± 1‰ of the enriched $\delta^{18}O$ values in the pore ice, assuming a $\delta^{18}O$/altitude effect of 0.6 ‰/100 m (32) and $\delta^{18}O$/temperature sensitivity of 0.7 ± 0.1 ‰/°C (23). Temperatures ~0.2° to ~3° warmer than present and/or phase changes within the sediment account for the remaining $\delta^{18}O$ enrichment (SI includes full details). The deuterium excess and ^{17}O excess values are consistent with modern precipitation and do not indicate alteration (Table S11).

Terrestrial plant macrofossils are abundant in both samples and preserve a record of the vegetation that occupied northwestern Greenland during ice-free intervals (Figs. 3A-J, S4-7). The upper sample includes twigs (possibly including *Empetrum*), moss leaves and stems of *Tomentypnum nitens, Polytrichum juniperinum,* and sclerotia of the fungus *Cenococcum geophilum* (Figs. 3A-H, S4-6), which are consistent with a tundra ecosystem, but could co-exist with boreal forest (9). In the lower sample, macrofossils such as bryophyte stems are present (Fig 3I-J, S7), but not as well preserved, and thus difficult to identify. Mixed woody tissue from the upper and lower samples yield $\delta^{13}C$ ratios of -26.7 ± 0.1‰ and -29.6 ± 0.1‰, $\delta^{15}N$ ratios of 2.4 ± 0.8‰ and -2.3 ± 0.8‰, and C/N ratios ranging from 15.0-23.0 and 47.4-53.5, respectively, which are consistent with tundra as well as boreal vegetation (Table S12) (33). A twig from the upper sample yielded a radiocarbon age >50 ^{14}C kyr (Table S13).

Well-preserved leaf waxes in Camp Century basal sediment resemble those of modern Greenland tundra ecosystems. Concentrations are higher in the upper sample (Fig 3K, Tables S14-15). Both samples contain C_{20} to C_{32} *n*-alkanoic acids with minimal interference from unsaturated compounds and a high even-to-odd chain length index (>3.45), indicating minimal post-depositional alteration. The *n*-alkanoic acids are dominated by C_{24}, similar to modern lake sediments on Greenland and soils in boreal forest regions of Canada (34, 35). The mid-chain *n*-alkanes (C_{21} to C_{25}) have a low odd-to-even chain length index (≤1.0) and co-elute with an unidentified complex mixture, likely derived from hydrocarbon-based drilling fluid (Fig S8). Long-chain *n*-alkanes (C_{27} to C_{33}) have a high odd-to-even chain length index (>4.5) and are dominated by C_{27} and C_{29}, similar to modern shrubs on Greenland (36).

Discussion

The Camp Century sub-glacial sediment provides a unique stratigraphic record of ice-free ecosystems and ice cover in Greenland. Plant macrofossils and lipid biomarkers in both samples are direct evidence for the preservation of terrestrial paleo-ecosystems beneath the ice sheet. The greatly enriched $\delta^{18}O$ of pore ice in both samples requires that precipitation fell at much lower elevations, demonstrating ice-sheet absence and possibly a warmer climate and/or phase changes in the sediment. Based on differences in stratigraphy, weathering, and $^{26}Al/^{10}Be$ ratios between the upper and lower sediment, and the lower diamicton IRSL minimum burial age (>0.7-1.4 Ma), this sedimentary sequence represents at least two episodes of sub-aerial exposure and subsequent burial. Abundant sub-horizontal ice lenses are present only in the lower diamicton,

which suggests an active permafrost environment before the emplacement of the upper diamicton unit. The non-conformable contact between the intermediate debris-rich ice layer and the overlying upper diamicton suggests a second glacial advance that incorporated and transported sediment and vegetation from a younger ice-free event.

The Camp Century lower diamicton, buried after 3.2 ± 0.4 Ma ($^{26}Al/^{10}Be$ maximum age) but before 0.7-1.4 Ma (IRSL minimum age), may derive from the growth of the GrIS during the Early Pleistocene (Fig 4). The cosmogenic $^{26}Al/^{10}Be$ limiting burial ages fit with the timing of GrIS expansion to the edge of the continental shelf at ~2.7 Ma (Fig 4E) (1, 6). The presence of extensive grain coatings and high solute concentrations in pore-ice are remnants of a weathered surface landscape (2, 15) (Fig 2). Given the burial age range, macrofossils and lipid biomarkers in the lower diamicton add to growing evidence that paleo-ecosystems from the Early Pleistocene, and perhaps earlier, are preserved both in present ice-free areas (7, 8) as well as below the GrIS (16). The lower diamicton represents the oldest terrestrial record for an ice-free ecosystem recovered beneath the GrIS.

Exposure of the Camp Century upper diamicton within the last 1.0 ± 0.1 Myr is consistent with paleoclimate records, including basal materials in other ice cores, which suggest a smaller or possibly absent GrIS within the last ~1 Myr. Ice-absence in the northwestern GrIS periphery at Camp Century since 1.0 ± 0.1 Myr agrees with the timing of bedrock exposure below the GrIS summit (<1.1 Ma) (10), which together mandate that much of Greenland was ice-free within the last 1.1 Myr (Fig 4G, Table S16). The maximum burial duration for the GISP2 bedrock and the Camp Century upper diamicton are consistent with GRIP basal ice ages (950-970 ka) (9, 19). These age constraints require that the GrIS was smaller during the last 1.1 Myr, most likely during a Pleistocene super-interglacial; however, the precise timing and extent remains uncertain. During MIS 31 (1.06-1.09 Ma) global mean sea level reached its Pleistocene maximum (37) and paleotemperatures in northeastern Siberia were elevated (38), consistent with a greatly reduced GrIS (Fig 4A-C). A smaller-than-present GrIS during the long MIS 11 (374-424 ka) interglacial is also possible as offshore records suggest a more ice-free and forested southern Greenland during this time (3, 4, 9) and sea-level records require significant reduction of the GrIS (39). In contrast, ice-core and geologic evidence (9, 12, 19–21, 23–25) along with modeling studies (26) suggest that the GrIS was mostly intact during MIS 5e (119-125 ka).

The similarity of $^{26}Al/^{10}Be$ burial histories between the Camp Century upper diamicton and GISP2 sub-glacial bedrock (10) suggests a similar history of ice cover and absence between the GrIS margin and interior (Fig S9, Table S16). The slightly higher $^{26}Al/^{10}Be$ (4.5 ± 0.3) in the Camp Century upper diamicton than GISP2 bedrock (4.1-4.2), and thus slightly shorter burial duration, is consistent with the ice-marginal position of Camp Century. Nevertheless, the similarity not only indicates GrIS presence for much of the Pleistocene, but also suggests at least one episode of greatly reduced ice-sheet extent, likely in response to prolonged interglacial warmth. For much of the Pleistocene, the GrIS persisted through interglacial periods while other northern hemisphere ice sheets vanished; however, our data show that the GrIS disappeared from Camp Century at some point in the last 1.1 million years. The sensitivity of the GrIS to past warming is critical for assessing future ice-sheet response to climate change and contribution to sea level-rise. Analysis of the basal silty ice and the remaining archive of sub-glacial sediment from Camp Century will further resolve the cryostratigraphy and how sediments were emplaced, as well as the sensitivity of the GrIS margin to past warming and the types of ecosystems that develop under warmer, ice-free conditions in Greenland.

Materials and Methods

Materials

The sub-glacial sediment from the Camp Century ice core was collected in 1966 (28). The sediment was stored frozen, initially at University at Buffalo from 1966 until it was transferred to Niels Bohr Institute (NBI), Copenhagen in 1994 and 1996. The samples are kept at -30°C as ~10 cm thick subsamples stored in individual glass jars. In the summer of 2019, two samples, 1059-4 and 1063-7, were cut at NBI using a dedicated cold-room hosted diamond-wire saw, designed for cutting heterogeneous material (40). Loose material from 1059-4 was kept as a replicate sample (1059-4 Debris).

Sedimentological description

Basal sediment was inventoried, photographed, and described in October 2019 in the NBI freezer. The dimensions and masses of each sub-sample were measured to determine the bulk density (~5% uncertainty). We refined the preliminary characterization of the sub-glacial sediment (29) by describing the granulometry, texture, clast shape, and presence of particular structures, such as ice-lenses or deformation features. Our observations and the presence of mixed lithologies indicate that these Camp Century sediments are probably glacial diamictons consisting of glacial and/or periglacial sediments reworked by subsequent ice advances after initial deposition. A full sediment description is in the Supplementary Information.

Sample processing

Sample material was sent frozen to the University of Vermont (UVM). We sub-sampled frozen fragments (~10 mg) of original samples for infrared stimulated luminescence (IRSL) and scanning electron microscopy including energy dispersive spectroscopy (SEM-EDS). Samples were thawed at 4°C inside sample bags. Pore-ice meltwater was decanted from sample bags directly into 50 mL plastic vials. Remaining sediment was transferred into clean, unused beakers, centrifuged, and then meltwater was decanted into 50 mL vials. Pore-ice melt samples were stored in 50 mL test tubes, capped, sealed, and refrigerated at 4°C.

Sediment was dried at 65°C, photographed, assigned a soil color, and measured for mass. Sediment was wet sieved with deionized water into <125, 125-250, 250-500, 500-850, 850-2000, and >2000 µm grain size fractions. During wet sieving, woody tissue and macrofossils were isolated using a dedicated disposable pipette, dried on a paper filter over a vacuum, and stored frozen. The 250-500 and 500-850 µm fractions were density separated using lithium polytungstate to isolate the felsic mineral fraction (<2.85 g/cm^3).

Major ion chemistry

Pore-ice meltwater was aliquoted by volume (1059-4: 4 mL; 1063-7: 0.5 mL) and massed. Samples were diluted to 10 mL (1059-4) and 8 mL (1063-7), re-massed, transferred to 10 mL syringes, and filtered through 0.45 µm nylon filters back into the initial vials. Major cations and anions were measured using atomic absorption spectroscopy (Perkin-Elmer PinAAcle 900H) and ion chromatography (Metrohm 883/863 Ion Chromatograph) in the Environmental Analysis Lab at Williams College. Si was measured with a Technicon Autoanalyzer II utilizing the reduction of silicomolybdate to “molybdenum blue” with ascorbic acid. Lab pH and alkalinity were determined using a Fisher Scientific 320 pH meter, a Radiometer-analytical TIM840 auto-titrator and double endpoint Gran titration.

SEM-EDS analyses of grain coatings

Thawed sample materials (~100 g) were sprinkled onto clean paper and embedded in epoxy (EPO-TEK 301). Epoxy plugs were polished using a decreasing grit size to 1 µm and carbon sputter-coated prior to analysis in BSE mode using a TESCAN VEGA3 Scanning Electron Microscope (SEM) coupled with an Oxford Instruments AZtec Elemental Mapping EDS in the

Geology Department at Middlebury College. EDS maps were acquired at 20 keV for a minimum of 3 minutes and tricolor plots generated using the Gatan digital micrograph 3.1 software.

Cosmogenic ^{10}Be and ^{26}Al

Quartz purification and beryllium and aluminum extraction were performed independently at UVM (250-500, 500-850 µm) and Lamont-Doherty Earth Observatory (LDEO), Columbia University (>2000 µm). At UVM, quartz from the felsic separates of the 250-500 and 500-850 µm fractions was purified using acid etches (41), and then Be and Al were isolated and extracted using standard procedures (42) specialized for low concentration samples (43). Two procedural blanks were prepared with the samples during extraction to estimate ^{10}Be and ^{26}Al backgrounds from laboratory sample processing and accelerator mass spectroscopy analysis. At LDEO, the >2000 µm samples were crushed, and quartz was isolated and mostly separated from feldspar by froth-flotation. The quartz fraction was subsequently leached in 1% HF / 3% HNO_3 on the shaker table. We followed LDEO procedures for low-level ^{10}Be and ^{26}Al analyses from quartz (10, 44).

^{10}Be/^{9}Be ratios in all samples and blanks were measured at the Center for Accelerator Mass Spectrometry, Lawrence Livermore National Laboratory (LLNL) and normalized to primary standard 07KNSTD3110 (assumed ^{10}Be/^{9}Be ratio: 2850×10^{-15}) (Tables S2) (45). At UVM, four blanks (~240 µg ^{9}Be) are included in the *in situ* blank correction: two processed side-by-side with samples in this project (664BLK and 664BLKX) and two from another batch of low-concentration samples from a separate project (BLK, BLKX, batch 662) processed in the same hood and analyzed together at LLNL. For samples prepared at UVM, we used an average blank ^{10}Be/^{9}Be ratio of $7.4 \pm 2.4 \times 10^{-16}$; subtracted the blank ratio from the sample ratios, and propagated uncertainties in quadrature (Table S3). At LDEO, four blanks (~187 µg ^{9}Be) are included, yielding an average ^{10}Be/^{9}Be ratio of $4.1 \pm 1.9 \times 10^{-16}$ (Table S4). Blank subtraction and error propagation were calculated using the UVM procedure.

^{27}Al/^{26}Al ratios in all samples and blanks were measured at the Purdue Rare Isotope Measurement (PRIME) Laboratory and normalized against primary standard KNSTD (assumed ratio: 1.818×10^{-12}) (Table S5) (46). For samples prepared at UVM, we calculated the blank correction by averaging the two batch blanks. To constrain the uncertainty, we used the precision based on counting statistics because the two blanks agreed more closely than statistically allowable. We used a blank ratio of $1.8 \pm 0.3 \times 10^{-15}$, subtracted the blank ratio from the sample ratios, and propagated uncertainties in quadrature (Table S6). We applied a consistent strategy for the LDEO samples, with two blanks (average $9.8 \pm 0.8 \times 10^{-16}$) (Table S7).

Infrared Optically Stimulated Luminescence (IRSL)

Luminescence dating estimates the time since sediment was last exposed to light, which resets the luminescence signal (47). Samples were sent frozen to the Utah State University Luminescence Lab. The outer 2 mm of each sample was shaved off to remove light-exposed sediments and processed to isolate the 150-350 µm of the quartz and potassium feldspar fractions. 1059-4 (USU-3195) produced little natural luminescence signals, indicating bleaching by light exposure during storage and subsampling. Measurements of the quartz fraction of 1063-7 (USU-3196) indicated that the natural signal was saturated and beyond dating range. All remaining measurements were conducted on the feldspar fraction of 1063-7.

IRSL measurements followed the single-aliquot regenerative-dose method for feldspars (48) and measures to reduce effects of anomalous fading (loss of signal with time). The first analyses followed the high temperature post-infrared IRSL method with IR stimulation at 225 ºC ($p\text{-}IRSL_{225}$) (49, 50) and included fading correction (47, 51). The second measurements utilized a modified pIRSL protocol with multiple elevated temperatures (MET-pIRSL (52) where equivalent dose (De) values were calculated at progressively higher temperatures (50-300 ºC, at 50 ºC

temperature steps). Dose-rate values for each sample were determined using ICP-MS and ICP-AES on sub-samples from each core segment (Table S9).

Results from both IRSL measurement techniques are presented in Table S10 and De distributions are presented in Figure S3. Dose-response measurements indicate that the natural luminescence signals were near or beyond saturation and results should be considered minimum age estimates. The fading corrected p-$IRSL_{225}$ results suggest the basal sample was last exposed to light at least 0.70 Myr and the MET p-$IRSL_{200, 250}$ results suggest the sample was deposited prior to 1.4 Ma. Supplemental Information includes a detailed IRSL methods.

Pore ice stable isotopes

We used established laser spectroscopy methods (53, 54), to analyze 1 mL aliquots of undiluted pore-ice meltwater for $\delta^{18}O$, δD, and $\delta^{17}O$ at the University of Washington. Samples were calibrated against in-house reference waters previously calibrated against VSMOW and SLAP, using GISP as a quality standard. The reference waters used were SW (Seattle Water) and VW (Vostok Water), with WW (West Antarctic water) used as a quality check. WW has δD, $\delta^{17}O$, and $\delta^{18}O$ similar to that of modern Greenland summit snow. Values for all standards, and details of the measurement and calibration procedure, are given in (53–55).

Macrofossil and pollen extraction and examination

Separate size fractions were rinsed with distilled water into a clean petri dish and examined under a dissectoscope (10-60X) and then at 100-200X for moss leaf detail and photos at LDEO. Macrofossils were better preserved and more easily identified in 1059-4 than 1063-7. Pollen extraction and examination used standard techniques using screens of 7 µm and 150 µm, acetolysis, and mounting in silicone oil (56). No pollen was found.

Organic geochemistry

Bulk woody tissue was analyzed for $\delta^{15}N$, $\delta^{13}C$, total organic nitrogen (TON), and carbon (TOC) at the University of Washington using continuous-flow mass spectrometry. Samples were flash combusted at 1000 °C with excess oxygen in a Costech ECS 4010 Elemental Analyzer following established methods (57, 58). TON and TOC are calibrated with a glutamic acid standard with known N and C concentrations. Internal laboratory reference materials (glutamic acid GA1 ($\delta^{13}C$ = -28.3 ‰, $\delta^{15}N$ = -4.6‰), GA2 ($\delta^{13}C$ = -13.7 ‰, $\delta^{15}N$ = -5.7 ‰), and Salmon ($\delta^{13}C$ = -21.33 ‰, $\delta^{15}N$ = +11.3‰) were interspersed with samples for calibration. All data are on to the Air-N_2 scale, for $\delta^{15}N$, and to the VPDB scale, for $\delta^{13}C$. Precision and accuracy are determined for each run using one of the three references as an unknown.

Replicate TOC and TON analyses of bulk woody tissue were performed at the UVM Environmental Stable Isotope Facility by combusting samples in sealed tin capsules and analyzing the gas released in a CE Instruments NC 2500 elemental analyzer calibrated with OAS B-2150 (6.72% C, 0.50% N) and NIST Peach Leaves (46.34% C, 2.9 % N). The precision of the analyzer is ~1% of the quantity measured for TOC, and ~0.5% for TON.

Radiocarbon

A twig and aliquot of woody tissue from 1059-4 were analyzed for $^{14}C_{organic}$ at the Keck-Carbon Cycle AMS, University of California Irvine. Samples (plus secondary standards and blanks of known-age and ^{14}C-free wood) were sonicated in acetone, methanol, and MQ water to remove possible contamination from drilling fluid and then treated with acid-base-acid (1N HCl and 1N NaOH, 75°C) prior to combustion. ^{14}C-dead blanks and standards covering a range of sizes were prepared and run with the two samples to estimate the masses of the modern and

dead blanks. One sigma uncertainty values for the resulting blank corrections are based on observed blank scatter within and between runs and are ±50% for samples <100 µg. The 1059-4 wood sample disintegrated during the solvent sonication and only a small mass of sample (56 µg) was analyzed, which may have resulted in modern ^{14}C contamination that yielded a finite age.

Lipid biomarkers

We extracted, purified, and analyzed the *n*-alkanoic acids and *n*-alkanes from the <125 µm fraction in the University at Buffalo Organic and Stable Isotope Biogeochemistry Lab following published procedures (59). We extracted free lipids from homogenized, dried samples on an Accelerated Solvent Extractor (Dionex ASE-200) using methylene chloride (DCM): methanol 9:1 (v:v), flushed three times at 10 minutes each. We added cis-eicosenoic acid and hexatriacontane internal standards to each sample, and purified the samples using flash column chromatography. We methylated the acid fraction with acidified methanol at 60°C for 8 hours. We quantified the resulting fatty acid methyl ester (FAME) peak areas on a Thermo Trace 1310 Gas Chromatograph with flame ionization detector. We converted peak areas to compound mass by comparison with an external calibration curve established for a C_{28} FAME standard (for FAMEs) and a C_{27} alkane standard (for alkanes), and normalized compound mass by dry mass of the extracted sediment.

Acknowledgments

We thank J. Racela, A.J. Schauer, O. Cowling, B. Buck, J. Goes, B. Linsley, M. Kirk, and L. Williamson for analytic assistance, and the Geology Department at Middlebury College for SEM-EDS access. Ice core samples curated by the University of Copenhagen since 1994. We thank the editor and two anonymous reviewers for constructive comments. Funding support: Gund Institute for Environment (Christ, Bierman), NSF-EAR 1735676 (Bierman), NASA/GISS and LDEO (Peteet), Belgian FNRS – FRFC grant no. 2.4601.12F (Tison), NSF-EAR 1652274 (Thomas). Prepared by LLNL under Contract DE-AC52-07NA27344; LLNL-JRNL-811066 (Hidy).

References

1. H. C. Larsen, *et al.*, 7 million years of glaciation in Greenland. *Science* **264**, 952–955 (1994).
2. P. R. Bierman, J. D. Shakun, L. B. Corbett, S. R. Zimmerman, D. H. Rood, A persistent and dynamic East Greenland Ice Sheet over the past 7.5 million years. *Nature* **540**, 256–260 (2016).
3. A. de Vernal, C. Hillaire-Marcel, Natural Variability of Greenland Climate, Vegetation, and Ice Volume During the Past Million Years. *Science* **320**, 1622–1625 (2008).
4. A. V. Reyes, *et al.*, South Greenland ice-sheet collapse during Marine Isotope Stage 11. *Nature* **510**, 525–528 (2014).
5. R. G. Hatfield, *et al.*, Interglacial responses of the southern Greenland ice sheet over the last 430,000 years determined using particle-size specific magnetic and isotopic tracers. *Earth Planet. Sci. Lett.* **454**, 225–236 (2016).
6. P. C. Knutz, *et al.*, Eleven phases of Greenland Ice Sheet shelf-edge advance over the past 2.7 million years. *Nat. Geosci.* **12**, 361–368 (2019).
7. S. Funder, *et al.*, Late Pliocene Greenland - The Kap København Formation in North Greenland. *Bull. Geol. Soc. Denmark* **48**, 117–134 (2001).
8. O. Bennike, *et al.*, Early Pleistocene sediments on Store Koldewey, northeast Greenland. *Boreas* **39**, 603–619 (2010).

9. E. Willerslev, *et al.*, Ancient biomolecules from deep ice cores reveal a forested southern Greenland. *Science* **317**, 111–114 (2007).

10. J. M. Schaefer, *et al.*, Greenland was nearly ice-free for extended periods during the Pleistocene. *Nature* **540**, 252–255 (2016).

11. P. R. Bierman, *et al.*, Preservation of a Preglacial Landscape Under the Center of the Greenland Ice Sheet. *Science* **344**, 402–405 (2014).

12. NEEM Community Members, Eemian interglacial reconstructed from a Greenland folded ice core. *Nature* **493**, 489–494 (2013).

13. A. Tripati, D. Darby, Evidence for ephemeral middle Eocene to early Oligocene Greenland glacial ice and pan-Arctic sea ice. *Nat. Commun.* **9**, 1–11 (2018).

14. K. Blake-Mizen, *et al.*, Southern Greenland glaciation and Western Boundary Undercurrent evolution recorded on Eirik Drift during the late Pliocene intensification of Northern Hemisphere glaciation. *Quat. Sci. Rev.* **209**, 40–51 (2019).

15. A. J. Christ, *et al.*, The Northwestern Greenland Ice Sheet During The Early Pleistocene Was Similar To Today. *Geophys. Res. Lett.* **47**, 1–9 (2020).

16. A. A. Garde, *et al.*, Pleistocene organic matter modified by the Hiawatha impact, northwest Greenland. *Geology* **48**, 867–871 (2020).

17. A. De Vernal, P. J. Mudie, Late Pliocene to Holocene palynostratigraphy at ODP Site 645, Baffin Bay. *Proc., Sci. results, ODP, Leg 105, Baffin Bay Labrador Sea* **105**, 387–399 (1989).

18. A. De Vernal, P. J. Mudie, Pliocene and Pleistocene palynostratigraphy at ODP Sites 646 and 647, eastern and southern Labrador Sea. *Proc., Sci. results, ODP, Leg 105, Baffin Bay Labrador Sea* **105**, 401–422 (1989).

19. A. M. Yau, M. L. Bender, T. Blunier, J. Jouzel, Setting a chronology for the basal ice at Dye-3 and GRIP: Implications for the long-term stability of the Greenland Ice Sheet. *Earth Planet. Sci. Lett.* **451**, 1–9 (2016).

20. M. Suwa, J. C. von Fischer, M. L. Bender, A. Landais, E. J. Brook, Chronology reconstruction for the disturbed bottom section of the GISP2 and the GRIP ice cores: Implications for Termination II in Greenland. *J. Geophys. Res. Atmos.* **111**, 1–12 (2006).

21. M. L. Bender, E. Burgess, R. B. Alley, B. Barnett, G. D. Clow, On the nature of the dirty ice at the bottom of the GISP2 ice core. *Earth Planet. Sci. Lett.* **299**, 466–473 (2010).

22. A. Strunk, *et al.*, One million years of glaciation and denudation history in west Greenland. *Nat. Commun.* **8**, 1–8 (2017).

23. S. J. Johnsen, *et al.*, Oxygen isotope and palaeotemperature records from six Greenland ice-core stations: Camp Century, Dye-3, GRIP, GISP2, Renland and NorthGRIP. *J. Quat. Sci.* **16**, 299–307 (2001).

24. A. Svensson, *et al.*, Annual layering in the NGRIP ice core during the Eemian. *Clim. Past* **7**, 1427–1437 (2011).

25. E. J. Colville, *et al.*, Sr-Nd-Pb isotope evidence for ice-sheet presence on Southern Greenland during the last interglacial. *Science* **333**, 620–623 (2011).

26. M. M. Helsen, W. J. Van De Berg, R. S. W. Van De Wal, M. R. Van Den Broeke, J. Oerlemans, Coupled regional climate-ice-sheet simulation shows limited Greenland ice loss during the Eemian. *Clim. Past* **9**, 1773–1788 (2013).

27. A. Aschwanden, *et al.*, Contribution of the Greenland Ice Sheet to sea level over the next millennium. *Sci. Adv.* **5** (2019).

28. B. L. Hansen, C. Langway, Deep core drilling in ice and core analysis at Camp Century,

Greenland, 1961-66. *Antarct. J. United States* **Sept-Oct**, 207–208 (1966).

29. J. Fountain, T. M. Usselman, J. Wooden, C. C. Langway, Evidence of the bedrock beneath the Greenland ice sheet near Camp Century, Greenland. *J. Glaciol.* **27**, 193–197 (1981).

30. D. M. Harwood, Do Diatoms beneath the Greenland Ice Sheet Indicate Interglacials Warmer than Present? *Arctic* **39**, 304–308 (1986).

31. L. B. Corbett, *et al.*, Cosmogenic 26Al/10Be surface production ratio in Greenland. *Geophys. Res. Lett.* **44**, 1350–1359 (2017).

32. B. M. Vinther, *et al.*, Holocene thinning of the Greenland ice sheet. *Nature* **461**, 385–388 (2009).

33. S. M. Schaeffer, E. Sharp, J. P. Schimel, J. M. Welker, Soil-plant N processes in a High Arctic ecosystem, NW Greenland are altered by long-term experimental warming and higher rainfall. *Glob. Chang. Biol.* **19**, 3529–3539 (2013).

34. E. K. Thomas, J. P. Briner, J. J. Ryan-Henry, Y. S. Huang, A major increase in winter snowfall during the middle Holocene on western Greenland caused by reduced sea ice in Baffin Bay and the Labrador Sea. *Geophys. Res. Lett.* **43**, 5302–5308 (2016).

35. A. Bakkelund, T. J. Porter, D. G. Froese, S. J. Feakins, Net fractionation of hydrogen isotopes in n-alkanoic acids from soils in the northern boreal forest. *Org. Geochem.* **125**, 1–13 (2018).

36. M. A. Berke, A. Cartagena Sierra, R. Bush, D. Cheah, K. O'Connor, Controls on leaf wax fractionation and δ2H values in tundra vascular plants from western Greenland. *Geochim. Cosmochim. Acta* **244**, 565–583 (2019).

37. K. G. Miller, *et al.*, Cenozoic sea-level and cryospheric evolution from deep-sea geochemical and continental margin records. *Sci. Adv.* **6**, 1–15 (2020).

38. M. Melles, *et al.*, 2.8 Million Years of Arctic Climate. *Science* **337**, 315–320 (2012).

39. A. Dutton, *et al.*, Sea-level rise due to polar ice-sheet mass loss during past warm periods. *Science (80-.).* **349** (2015).

40. J. L. Tison, Diamond wire-saw cutting technique for investigating textures and fabrics of debris-laden ice and brittle ice. *J. Glaciol.* **40**, 410–414 (1994).

41. C. P. Kohl, K. Nishiizumi, Chemical isolation of quartz for measurement of in-situ - produced cosmogenic nuclides. *Geochim. Cosmochim. Acta* **56**, 3583–3587 (1992).

42. L. B. Corbett, P. R. Bierman, D. H. Rood, An approach for optimizing in situ cosmogenic 10Be sample preparation. *Quat. Geochronol.* **33**, 24–34 (2016).

43. J. D. Shakun, *et al.*, Minimal East Antarctic Ice Sheet retreat onto land during the past 8 million years. *Nature* **558**, 284–287 (2018).

44. J. M. Schaefer, *et al.*, High-Frequency Holocene Glacier Fluctuations in New Zealand Differ from the Northern Signature. *Science* **324**, 622–625 (2009).

45. K. Nishiizumi, *et al.*, Absolute calibration of 10Be AMS standards. *Nucl. Instruments Methods Phys. Res. Sect. B Beam Interact. with Mater. Atoms* **258**, 403–413 (2007).

46. K. Nishiizumi, Preparation of 26Al AMS standards. *Nucl. Instruments Methods Phys. Res. Sect. B Beam Interact. with Mater. Atoms* **223**–**224**, 388–392 (2004).

47. D. J. Huntley, M. Lamothe, Ubiquity of anomalous fading in K-feldspars and the measurement and correction for it in optical dating. *Can. J. Earth Sci.* **38**, 1093–1106 (2001).

48. J. Wallinga, A. Murray, A. Wintle, The single-aliquot regenerative-dose (SAR) protocol

applied to coarse-grain feldspar. *Radiat. Meas.* **32**, 529–533 (2000).

49. K. J. Thomsen, A. S. Murray, M. Jain, L. Bøtter-Jensen, Laboratory fading rates of various luminescence signals from feldspar-rich sediment extracts. *Radiat. Meas.* **43**, 1474–1486 (2008).

50. J. P. Buylaert, A. S. Murray, K. J. Thomsen, M. Jain, Testing the potential of an elevated temperature IRSL signal from K-feldspar. *Radiat. Meas.* **44**, 560–565 (2009).

51. M. Auclair, M. Lamothe, S. Huot, Measurement of anomalous fading for feldspar IRSL using SAR. *Radiat. Meas.* **37**, 487–492 (2003).

52. B. Li, Z. Jacobs, R. G. Roberts, S. H. Li, Review and assessment of the potential of post-ir irsl dating methods to circumvent the problem of anomalous fading in feldspar luminescence. *Geochronometria* **41**, 178–201 (2014).

53. E. J. Steig, *et al.*, Calibrated high-precision 17O-excess measurements using cavity ring-down spectroscopy with laser-current-tuned cavity resonance. *Atmos. Meas. Tech.* **7**, 2421–2435 (2014).

54. A. J. Schauer, S. W. Schoenemann, E. J. Steig, Routine high-precision analysis of triple water-isotope ratios using cavity ring-down spectroscopy. *Rapid Commun. Mass Spectrom.* **30**, 2059–2069 (2016).

55. S. W. Schoenemann, A. J. Schauer, E. J. Steig, Measurement of SLAP2 and GISP δ17O and proposed VSMOW-SLAP normalization for δ17O and 17Oexcess. *Rapid Commun. Mass Spectrom.* **27**, 582–590 (2013).

56. K. Faegri, J. Iversen, *Textbook of Pollen Analysis*, 4th Ed. (John Wiley and Sons, 1989).

57. A. Barrie, J. E. Davies, A. J. Park, C. T. Workman, Continuous-flow stable isotope analysis for biologists. *Spectroscopy* **4**, 42–52 (1989).

58. D. J. Verardo, P. N. Froelich, A. McIntyre, Determination of organic carbon and nitrogen in marine sediments using the Carlo Erba NA-1500 Analyzer. *Deep. Res.* **37**, 157–165 (1990).

59. E. K. Thomas, K. V. Hollister, A. A. Cluett, M. C. Corcoran, Reconstructing Arctic precipitation seasonality using aquatic leaf wax δ2H in lakes with contrasting residence times. *Paleoceanogr. Paleoclimatology* **35**, e2020PA003886 (2020).

60. P. H. Blard, M. Lupker, M. Rousseau, J. Tesson, Two MATLAB programs for computing paleo-elevations and burial ages from paired-cosmogenic nuclides. *MethodsX* **6**, 1547–1556 (2019).

Figures and Tables

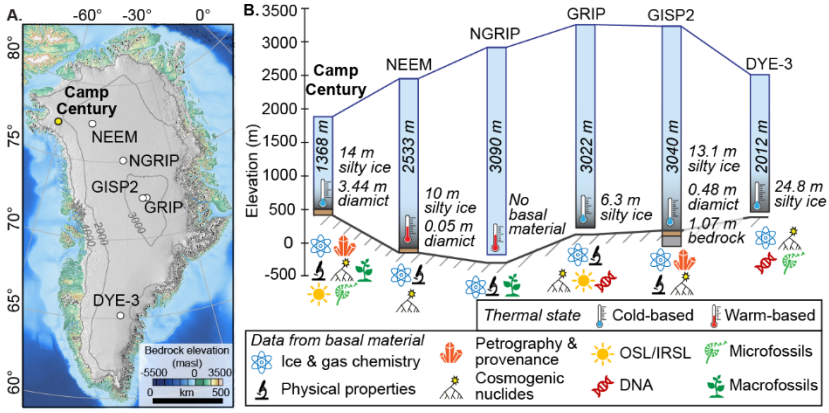

Figure 1. Greenland ice cores and basal materials. (A) Ice core locations (circles) shown with the bedrock topography and ice surface 1000 m elevation contours (light gray). (B) Ice core glacier ice thickness (to scale) above the bedrock elevation (dark gray line), basal material thickness (exaggerated), and analyses of basal materials (symbols).

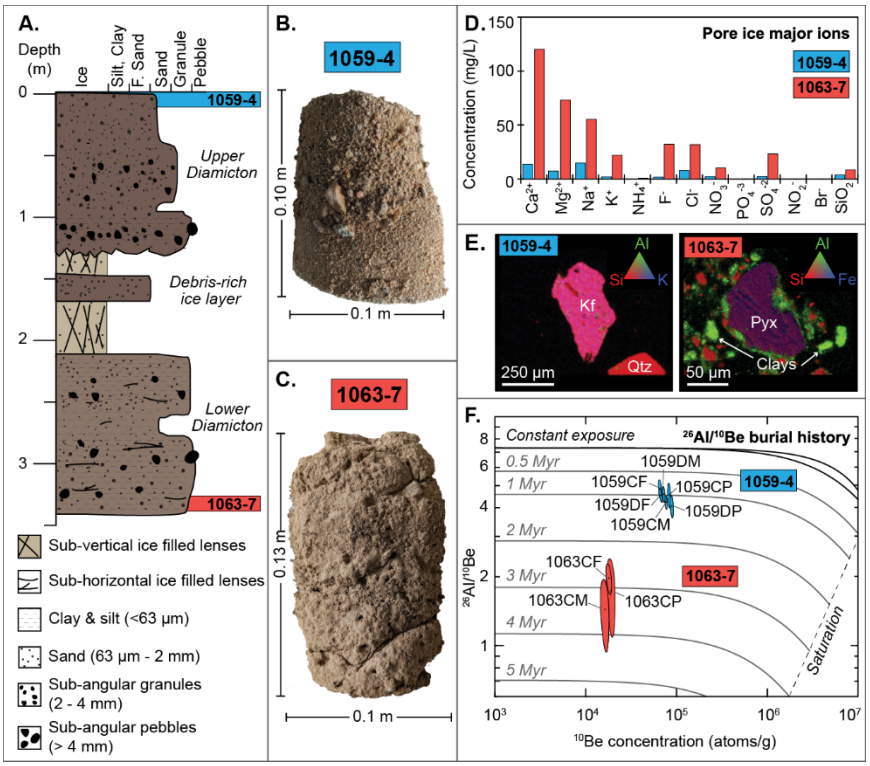

Figure 2. Camp Century basal sediment stratigraphy, weathering, and cosmogenic nuclide results. (A) sediment description showing sample intervals. Core sample photographs of (B)1059-4 and (C) 1063-7. (D) Pore-ice major ion chemistry and (E) representative SEM-EDS analysis of mineralogy of the diamictons; Kf – potassium feldspar, Qtz – quartz, Pyx – pyroxene. (F) ^{26}Al and ^{10}Be two-isotope plot showing constant surface exposure (black line) and burial isochrons (light gray); created using (60).

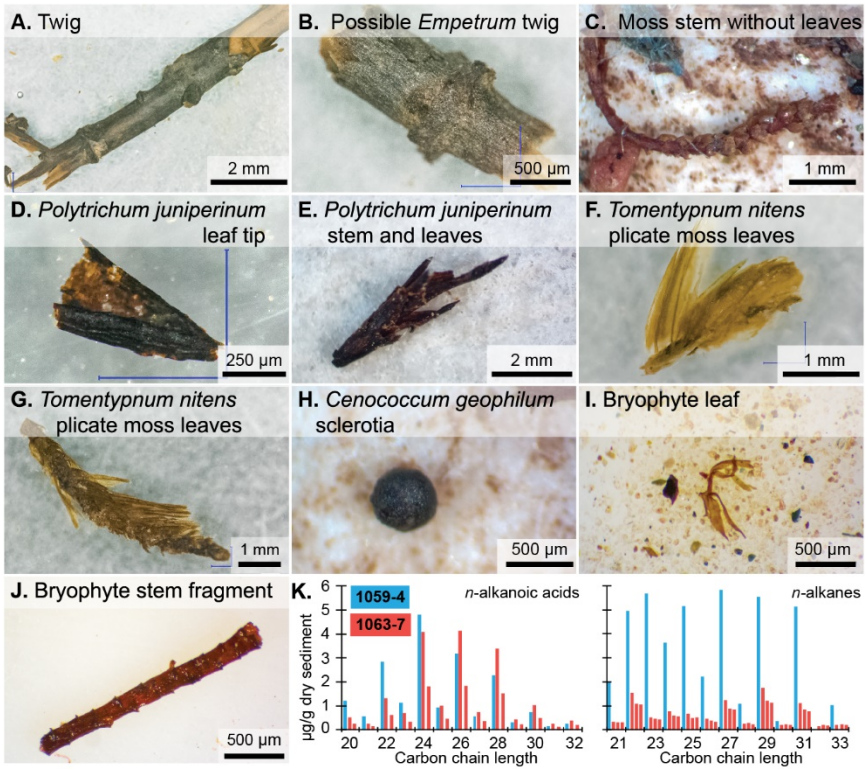

Figure 3. Macrofossil micrographs and leaf wax concentrations. Micrographs of macrofossils recovered in (A-H) the upper diamicton and (I-J) the lower diamicton. (K) Leaf wax concentrations of *n*-alkanoic acids and alkanes; multiple columns correspond to replicate analyses.

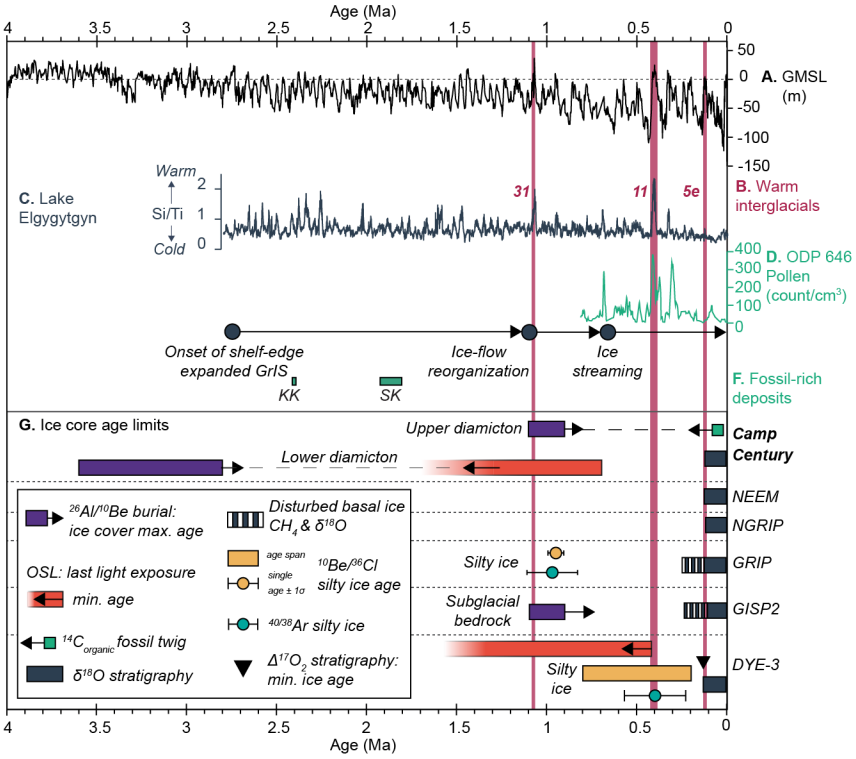

Figure 4. Paleoclimate and Greenland ice core age constraints since 4 Ma. (A) global mean sea level; dashed black line marks today (37). (B) Pleistocene super-interglacials since 1.1 Ma (pink columns). (C) Si/Ti paleotemperature proxy from Lake El'gygytgyn, Siberia (38). (D) Total minus bisaccate pollen concentration counts in ODP Site 646, Labrador Sea (3). (E) Changes in GrIS behavior in Melville Bay, west Greenland (6); (F) Green boxes: fossiliferous deposits; KK – Kap København, SK – Store Koldewey (7, 8). (G) Age constraints on materials from Camp Century and other Greenland ice cores (9, 10, 12, 20, 23). Dashed gray line shows bounding age constraints for the Camp Century subglacial sediment.